Atmos. Chem. Phys. Discuss., 11, 24467–24502, 2011
www.atmos-chem-phys-discuss.net/11/24467/2011/
doi:10.5194/acpd-11-24467-2011

Atmospheric Chemistry and Physics Discussions

Measurement-based modeling of bromine-induced oxidation of mercury above the Dead Sea

E. Tas[1,2], D. Obrist[3], M. Peleg[1], V. Matveev[1], X. Faïn[1], D. Asaf[1,2], and M. Luria[1]

[1]The Institute of Earth Sciences, The Hebrew University, Jerusalem, Israel
[2]Department of Environmental Sciences and Energy, The Weizmann Institute of Science, Israel
[3]Division of Atmospheric Sciences, Desert Research Institute, 2215 Raggio Parkway, Reno, Nevada, 89512, USA

Received: 13 June 2011 – Accepted: 8 August 2011 – Published: 31 August 2011

Correspondence to: E. Tas (eran.tas@weizmann.ac.il)

Published by Copernicus Publications on behalf of the European Geosciences Union.

Abstract

Atmospheric mercury depletion events (AMDEs) outside the polar regions – driven by high levels of reactive bromine species (RBS) – were observed recently in the warm Dead Sea boundary layer. Efficient oxidation of gaseous elemental mercury (GEM) under temperate conditions by RBS was unexpected considering that the thermal back dissociation reaction of HgBr, a proposed key mechanism, is more than 2.5 orders of magnitude higher under Dead Sea temperatures compared with polar temperatures. The goal of this study was to improve understanding of RBS-mercury interactions using numerical simulations based on a comprehensive measurement campaign performed at the Dead Sea during summer 2009.

Results demonstrate a high efficiency and central role of BrOx (i.e., Br + BrO) for AMDEs at the Dead Sea, with relative contributions for GEM depletion of more than ~90 %. BrO was found to be the dominant oxidant with relative contribution above 80 %. Best agreement between simulations and observations was achieved by applying rate constants for k_{Hg+Br} and k_{Hg+BrO} of 2.7×10^{-13} cm^3 molecule^{-1} s^{-1} and 1.5×10^{-13} cm^3 molecule^{-1} s^{-1}, respectively – indicating that k_{Hg+BrO} is higher than most reported values and that BrO is a more efficient oxidant than Br in the ozone-rich atmosphere (i.e., for [BrO]/[Br] >2). This further explains why the efficiency of GEM oxidation by reactive bromine species at the Dead Sea doesn't critically depend on Br and, therefore, is comparable to the efficiency in polar regions even under much higher temperatures. These findings also support the hypothesis identified in a previous study, that Br-induced GEM depletion can be important above oceans in the mid-latitudes and tropics. In the presence of anthropogenic NO_2, RBS activity can lead to enhanced NO_3 formation, which then causes significant nighttime GEM depletion.

ACPD
11, 24467–24502, 2011

1 Introduction

Atmospheric mercury is a persistent and toxic global pollutant, and the major contributions of mercury loadings in remote locations are due to atmospheric deposition (Lu et al., 2001; Driscoll et al., 2007). Most atmospheric mercury generally occurs as elemental gaseous mercury (GEM; >95 %) – a form which is highly inert, has a low deposition velocity, and shows global lifetime of ∼1–2 years (Schroeder et al., 1998). Field measurements in polar regions, however, showed that GEM can be oxidized rapidly to reactive forms (reactive gaseous mercury: RGM; and particulate Hg: Hg_P) after polar sunrise, followed by rapid deposition to the surface. Schroeder et al. (1998) were the first to show that during such events, termed Atmospheric Mercury Depletion Events (AMDE), nearly complete depletion of GEM can occur within 24 h or less. There is now a growing body of observational evidence indicating that rapid AMDEs, and subsequent scavenging by aerosols and deposition to the surface, are widespread in polar regions and the marine sub-Arctic and Antarctic (Lindberg et al., 2002; Ebinghaus et al., 2002; Berg et al., 2003; Skov et al., 2004; Poissant and Pilote, 2003).

The oxidation of GEM during AMDEs is known to be caused by Br and BrO (i.e., BrOx), as well as other reactive halogen species (RHS) (Lu et al., 2001; Lindberg et al., 2001; Ariya et al., 2004; Brooks et al., 2006). As a result, AMDEs strongly correlate with ozone depletion events (ODEs) (Bottenheim et al., 1986). It is well known that reactive halogens also can exist outside of polar regions at temperate mid-latitude locations such as over salt lakes and in the marine boundary layer (MBL) (Hebestreit et al., 1999; Saiz-lopez et al., 2004). Due to the important role that reactive bromine species (RBS) play in GEM oxidation, several studies, including modeling, focused on interactions of RBS with atmospheric mercury in the polar region (Calvert and Lindberg, 2003; Skov et al. , 2004; Hedgecock et al., 2008; Xie et al., 2008), in the MBL at mid-latitudes (Hedgecock and Pirrone, 2001, 2004; Hedgecock et al., 2003, 2005; Holmes et al., 2006, 2008, 2009), and in urban areas (Shon et al., 2005). For example, using an atmospheric chemistry model, Holmes et al. (2006) calculated a global

ACPD
11, 24467–24502, 2011

chemical lifetime of atmospheric mercury of 0.5–1.7 years against oxidation by Br, implying that Br is a significant oxidant of GEM on a global scale. Holmes et al. (2009) further indicated that oxidation of GEM by Br accounts for 35–60 % of the MBL reactive gaseous mercury source, with most of the remainder contributed by oxidation of GEM by ozone (5–20 %).

Currently, however, there are some significant uncertainties in regard to the reaction of RBS with Hg (see Ariya et al., 2008; Calvert and Lindberg, 2004; and Xie et al., 2008): reaction rates of Br and BrO with GEM are not well defined; it is not clear which is the dominant oxidant; Additionally, chemical pathways and consequent constituents of RGM formation are unclear. Additional uncertainties include oxidation rates by other oxidants – including halogens such as I and IO (Raofie et al., 2008), O_3, and OH (Xie et al., 2008 and references within) – as well as the temperature-dependence of most rate coefficients (Ariya et al. 2008; Xie et al., 2008).

Recently, it was observed that strong AMDEs are not limited to polar regions but also occur in the mid-latitudes under temperate conditions. Near-complete (up to ∼90 %) conversion of GEM to RGM was observed under the warm summer Dead Sea atmosphere (Peleg et al., 2007; Obrist et al., 2011). An important implication of the above studies was that bromine-driven $Hg^{(II)}$ formation could be a main source of atmospheric mercury deposition to the oceans. Dead Sea AMDEs correlated with high BrOx and were unexpected given that the kinetics of BrOx with GEM are highly temperature dependent (Goodsite, 2004).

The objective of the present study is to improve understanding of the Br-Hg interaction – particularly its dependence on temperature, by combining results obtained from a comprehensive measurement campaign performed at the Dead Sea during summer 2009 with detailed modeling analysis. Due to the elevated $[Br^-]$ and $[Br^-]/[Cl^-]$ ratio of the seawater (Niemi et al., 1997), low pH (<6; Tas et al., 2005) and moderate anthropogenic pollution (Tas et al., 2005), extremely high levels of BrO are formed almost daily at the Dead Sea (e.g., Tas et al. 2006). Due to the high BrO levels and moderate anthropogenic pollution, the Dead Sea provides excellent conditions for studying the

ACPD
11, 24467–24502, 2011

interaction of RBS with atmospheric mercury at mid-latitudes. We used the MECCA box model (Sander et al., 2005) heterogeneous mechanism, focusing on identifying reaction rates of BrO and Br with GEM, the relative importance of BrOx and other oxidants, and oxidation sensitivity to temperature and anthropogenic conditions. Our simulations built upon extensive atmospheric chemistry characterization at the Dead Sea, as described by several studies (Hebestreit et al., 1999; Matveev et al., 2001; Tas et al., 2005, 2006, 2008; Peleg et al., 2007; Smoydzin and von Glasow, 2009).

2 Experimental

2.1 Field measurements

Model simulations presented in this work are based on a comprehensive measurement campaign that took place at Ein Bokek, Israel (latitude 31.20° N, longitude 35.37° E) on the shore of the Dead Sea, between 29 June and 28 July 2009. Measurements are described in detail in Obrist et al. (2011), and additional details are found in Matveev et al. (2001) and Tas et al. (2005). Measurements included speciated atmospheric mercury (GEM, RGM, and Hg_P) using Tekran Model 2537, Model 1130, and Model 1135 analyzers (Tekran Inc.; Toronto, Canada). Measurements also included O_3 (TEII, Model 49C), NO-NO_x (TEII, Model 42i), SO_2 (TEII, Model 43C), CO (TEII, Model 48i), particulate sulfates (TEII, Model 5020i), and meteorological conditions including wind speed and direction, temperature, relative humidity, barometric pressure, and solar radiation. Relative humidity (RH) is a critical parameter regulating Br_2 release from Dead Sea water (Obrist et al., 2011). Therefore, we use RH' for measured RH, noting that RH' was likely lower than actual RH directly above the sea surface as measurements were taken about 17 m above the water surface and 25 m inland.

The long-path differential optical absorption spectroscopy (LP-DOAS) technique (model HMT DOAS Measuring System, Hoffmann Messtechnik, Rauensberg, Germany) was employed to quantify BrO (detection limit generally <3 pptv), O_3 (detection

ACPD
11, 24467–24502, 2011

limit generally <7.3 ppbv), and NO_2 (detection limit generally <0.5 ppbv). The LP-DOAS system (Model HMT DOAS Measuring System; Hoffmann Messtechnik GmbH, Rauensberg, Germany) was placed in the top floor of an air-conditioned hotel room (same location as above instruments), and the DOAS reflector mirror was situated at the eastern side of an evaporation ponds directly above the water surface, resulting in an 11.8 km light path traveling over the Dead Sea water. Details of the DOAS system and signal retrieval are described in Stutz and Platt (1996) and Peleg et al. (2007).

2.2 Model description

The model used in this analysis is the comprehensive heterogeneous MECCA box model (Sander et al., 2005). MECCA includes an explicit kinetic heterogeneous chemical mechanism, accounting for gas and aqueous phase reactions and heterogeneous reactions for two aerosol modes. In the gas phase, species are subjected to photochemical decomposition and dry deposition, while aerosol processes include both scavenging and new particle formation. Gas-aerosol partitioning is performed by MECCA based on Henry's law and kinetic limitations for coarse soluble and accumulation soluble aerosol modes. The O-H-C-N-S-Cl-Br-I chemical mechanism includes 186 gas phase reactions capturing 58 photolysis reactions, 266 aqueous reactions, and 154 heterogeneous reactions based on the default MECCA mechanism (http://www.mpch-mainz.mpg.de/~sander/messy/mecca/). The mercury chemical mechanism was added to the model for gas phase (Supplement Table 1), aqueous (Supplement Table 2), aqueous equilibrium (Supplement Table 3), and heterogeneous reactions (Supplement Table 4) in sea salt and sulphate aerosols. Photolysis rate coefficients are calculated by MECCA using the method described in Landgraf and Crutzen (1998).

The initial sea salt aerosol composition was based on the Dead Sea water composition accounting for Br^- and Cl^- concentrations, as reported by Tas et al. (2005). In MECCA, the averaged mass transfer coefficient for each aerosol mode is based on integration over a lognormal shape distribution of the particle radius, for each aerosol

ACPD
11, 24467–24502, 2011

mode (Kerkweg et al., 2007). Dependence of average sea salt aerosol number concentrations on wind speed was taken into account using Eq. (4) in Gong et al. (1997) on five-minute time resolution. Average sulphate aerosol number concentrations were determined based on in situ measurements, using reported densities (Karg et al., 1995) and radius dependency on RH (Yue, 1979).

2.3 Model simulations

Model simulations were based on a previous modeling study that described RBS formation and interaction with GEM at the Dead Sea using the same measurement campaign data (Obrist et al., 2011). This study showed that reactive bromine production via aerosols is limited to relative humidity (RH') of less than 28 %. Therefore, aerosol chemistry in our simulations was activated only for RH' above 28 %. The previous study shows that, in agreement with the study by Smoydzin and von Glasow (2009) direct release of bromine from seawater needs to be included in the model to accurately simulate observations, and an additional source representing direct Br_2 release from the seawater was included in our model, as described in Obrist et al. (2011).

All simulations were updated on a 15-min. time resolution using measured temperature; RH' (averaged at ~37 °C and 33 %); wind speeds; boundary layer height; and fluxes for NO, NO_2, SO_2, and 13 different hydrocarbons species (based on HC measurements; see Tas et al., 2006) in order to reach the observed non-AMDE/ODE levels, as described in Tas et al. (2006). An O_3 flux was added at the end of the AMDE/ODE to reach the background measured O_3 concentrations. Similarly, a GEM flux was added to reach the measured GEM prior to and after occurrence of AMDE. GEM fluxes were added for half an hour after the end of AMDE and between 06:00 and 08:00 LT (JD = 201) as well as 07:30 and 08:00 LT (JD = 197) to reach measured background GEM levels, and exceptionally also between 07:30 and 13:30 LT (JD = 188; see Sect. 3.2). Boundary layer height was determined using a 1-D meteorological model (McNider and Pielke, 1981). Photolysis rate coefficients were calculated by the MECCA model, representing clear sky conditions for the Dead Sea.

ACPD
11, 24467–24502, 2011

Simulations were performed according to the above model description for measurement campaign days (Julian days 188, 197, 198, and 201) using different combinations for the reaction rates of Hg with Br and BrO (see detailed description in Table 1). Based on a literature review and sensitivity analysis (Sect. 3.2), simulations were based on low and high values of k_{Hg+Br}, with values of 2.7×10^{-13} cm ^{3} molecule^{-1} s^{-1} and $1.1 \times 10^{-12} \times (T/298)^{-2.37}$ cm^3 molecule^{-1} s^{-1} (termed "L_Br" and "H_Br", respectively). For k_{Hg+BrO}, we used values of $1. \times 10^{-15}$ and $5. \times 10^{-14}$ cm^3 molecule^{-1} s^{-1} (termed "L_BrO" and "M_BrO") and a value of $1.5. \times 10^{-13}$ cm ^{3} molecule^{-1}s^{-1} (termed "H_BrO"). "L_Br_H_BrO" led to best agreement with measurements and therefore is termed "BASE" simulation.

Additional simulations were performed for Julian days 188 and 201 and summarized in Table 1: Simulation "L_Br_H_BrO_HgOp" is identical to the "BASE" simulation, except that the reaction of BrO and Hg was assumed to yield only HgO(s), particulate HgO, which is completely removed from the system. Simulation "NOBROX" is identical to the "BASE" simulation, except that all direct reactions of Hg with BrO_X were switched off. Simulations "ONLYBROX" and "ONLYBR" are identical to the "BASE" simulation except that they include only BrO_X and Br as GEM oxidants, respectively. Simulation "HIGHSO_2" is identical to the "BASE" simulation except that the SO_2 flux was multiplied by a factor of two, resulting in maximum daily SO_2 concentrations higher by a factor of ~2.6. All the above reaction rates were calculated using summer Dead Sea temperatures (averaged at ~310 k). In addition, "WINTER" and "POLAR" simulations are identical to the "BASE" simulation, except that winter Dead Sea temperatures (averaged at ~294 k) and typical polar temperatures (averaged at 240 k) were used to calculate all mercury-involved reactions.

ACPD
11, 24467–24502, 2011

3 Results and discussion

3.1 Model verification

The primary, non-halogen gas phase oxidants of GEM in the urban and lower troposphere boundary layer are O_3, H_2O_2, and OH (Hedgecock et al., 2005; Holmes et al., 2009; Sillman et al., 2007; Spivakovsky et al., 2000). In the marine boundary layer and upper troposphere, halogens are presumed to be the dominant oxidants (Lin et al., 2006). Bromine is a major global sink for GEM, especially in the middle and upper troposphere where relatively cold temperatures suppress the thermal back-decomposition of the HgBr intermediate (Holmes et al., 2006). During AMDEs in the polar regions, RHS and particularly RBS dominate the rate of GEM depletion (e.g., Xie et al., 2008). During Dead Sea AMDE, GEM depletions are strongly linked to BrOx levels (Obrist et al., 2011), primarily due to the very high concentrations of RBS compared to other halogens. Additional considerations include generally low iodine species concentrations present when RBS are active (Zingler and Platt, 2005), together with the higher efficiency of GEM depletion by RBS, compared with other RHS.

Hence, our model was configured to include a detailed account of reactive bromine species formation, but it also includes multiphase chemical reactions involving chlorine and iodine reactive species (Sect. 2.2) and interaction of these species with mercury in the gas and liquid phase. The photochemistry was carefully evaluated in the model, based on measurements at the Dead Sea, in order to adequately describe the RBS-O_3-NO_Y interaction (Obrist et al., 2011).

The release of Br_2 into the gas phase has been shown to be highly sensitive to wind speed and RH at the Dead Sea (Sect. 2.3), and oxidation of GEM by Br is highly temperature sensitive (i.e., decreases with increasing temperature) due to the thermal back-reaction of HgBr (Goodsite et al., 2004). Therefore, we updated the model by the in situ measured temperature, wind speed, and RH'. The calculated boundary layer height also was taken into account by the model, although vertical and spatial gradients were shown to play only a minor role at the measurement site (Obrist et al., 2011).

ACPD
11, 24467–24502, 2011

Model evaluation based on the selected days showed relatively good agreement between measured and simulated BrO concentrations (see panel "a" in Figs. 1, 2 and Supplement Figs. 1 and 2), indicating that the model was successful in predicting BrO formation. The analysis in the present paper was mostly based on Julian days 188 and 201, which represent typical Dead Sea and polar regions BrO levels, respectively.

3.2 Reaction rates of GEM with Br and BrO

Previous studies (Goodsite et al., 2004; Ariya et al., 2002; Calvert and Lindberg, 2004; Peleg et al., 2007) indicated that GEM oxidation by Br predominates over oxidation by BrO, since theoretical kinetic calculations suggest that the reaction of BrO with Hg is endoergic and therefore unlikely to occur in the atmosphere (Tossell et al., 2003; Holmes et al., 2006; Shepler et al., 2007). Experimental studies, however, found conflicting data on the energetics of the species existing in the vapor over heated $HgO_{(s)}$ (Tossell et al., 2006). Overall, a wide range of values have been published during the last decade, suggesting that GEM oxidation by Br ranges between a high value of $1\times10^{-13}-3\times10^{-12}$ cm ^{3} molecule^{-1} s^{-1} (see Ariya et al., 2008 and references within) and lower oxidation rates by BrO of 10^{-13}–10^{-15} cm ^{3} molecule^{-1} s^{-1} (Raofie and Ariya, 2003). Recently, Xie et al. (2008) pointed out that model simulations could best reproduce the observed correlation between GEM and O_3 if rate constants for GEM oxidation by Br and BrO were in the magnitude of 3×10^{-13} and $\leq 1.0\times10^{-15}$ cm^3 molecule^{-1} s^{-1}, respectively.

We performed sensitivity analyses to calibrate the model configuration for the present study in respect to reaction rates of Br and BrO with GEM. Figures 1, 2, and Supplement Figs. 1 and 2, present measured and simulated GEM concentrations for the four simulation days. For JD = 188, GEM concentrations had to be constrained between 07:30 and 13:30 LT (Fig. 1c), as model simulations showed at this time too intense GEM depletions (Fig. 1b). The reason for this is unknown but could be explained by entrainment of GEM from areas where measured BrO_X concentrations were low. The figures show that measured GEM depletions could best be reproduced when

ACPD
11, 24467–24502, 2011

employing the "BASE" simulation ("LBr_HBrO"). For k_{Hg+BrO} values smaller than used in "BASE", (i.e., L_Br_M_BrO, L_Br_L_BrO, and H_Br_L_BrO), simulations yielded relatively good agreement only on days with high BrO levels (such as day 188 in Fig. 1) but significantly underestimated GEM depletions for days with lower BrO levels (Fig. 2 and Supplement Figs. 1 and 2). Panel a in these figures also presents [BrO]/[Br] ratios: low BrO levels are associated with higher O_3 levels resulting in high [BrO]/[Br] ratios. The simulations show that using k_{Hg+BrO} values smaller than used in "BASE" underestimates GEM depletions, particularly on the days with high [BrO]/[Br] ratios (Fig. 2 and Supplement Figs. 1 and 2). This implies that the rate constant of k_{Hg+BrO} is particularly important and should not be lower than the value used by the "BASE" case (i.e., $1.5. \times 10^{-13}$ cm^3 molecule^{-1} s^{-1}). In contrast, use of rate constants other than in the "BASE" simulation yielded significantly less underestimation of GEM depletion at low [BrO]/[Br], while for H_Br_L_BrO an overestimation of GEM depletion was obtained (due to a higher k_{Hg+Br} value; see Fig. 1). These results indicate that the combination of rates for k_{Hg+Br} and k_{Hg+BrO} as used in "BASE" could best account for the observed GEM depletion under Dead Sea conditions.

The possible contribution of other halogens to GEM oxidation is unlikely, especially at high BrO_X levels (see Sect. 3.1). In order to demonstrate that the good agreement between the measured GEM and "BASE" simulation was not influenced by overprediction of the gas phase HgO, which can then return back to $Hg^{(0)}$ via aerosol aqueous chemistry, the L_Br_H_BrO_HgO_P simulation was performed with all produced HgO from the reaction between BrO and GEM assumed as a gas phase product (Sect. 2.3). Figures 1 and 2 demonstrate that differences between the GEM diurnal profile for this simulation and the "BASE" simulation are insignificant, indicating that recovery of Hg via HgO scavenging by the aerosol is insignificant compared with Hg depletion.

Figure 3a presents the relationships between GEM, BrO, and O_3 by graphing GEM depletion per change in BrO (i.e., ΔGEM/ΔBrO) as a function of O_3, and only for ΔBrO>0. Using daytime values only, measured ΔGEM/ΔBrO is higher at higher O_3 levels. [Br]/[BrO] ratios are expected to anti-correlate with O_3 (e.g., Wayne et al., 1995;

ACPD
11, 24467–24502, 2011

Tas et al., 2008), and therefore oxidation of GEM by BrO is expected to increase at the expense of oxidation by Br for high O_3 levels (Xie et al., 2008). Figure 3a therefore implies that GEM oxidation by BrO predominates over oxidation by Br, in agreement with the model simulations in Figs. 1 and 2, and Supplement Figs. 1 and 2. The possibility that higher efficiency of GEM depletion for higher O_3 levels predominantly results from higher GEM associated with higher O_3 levels may be ruled out by the much sharper change in $\Delta\frac{\text{GEM}}{\Delta\text{BrO}}$ compared with GEM change for O_3 of ~30–60 ppb (Fig. 3a).

Figure 3b–d compares the measured results from panel a with simulated ΔGEM/ΔBrO for Julian days 188, 201, 198 and 197, using three different simulations. ΔGEM/ΔBrO is graphed as a function of [Br]/[BrO], which is analogous to O_3 levels in panel a. These results show that the distribution of ΔGEM/ΔBrO versus [Br]/[BrO] – and, hence, versus O_3 – is in relatively good agreement with measurements for the "BASE" simulation (Fig. 3b; i.e., L_Br_H_BrO), although ΔGEM/ΔBrO ratios tend to peak at somewhat lower O_3 levels compared to measurements. This may suggest that the ratio between the rate constants of GEM with BrO and Br (e.g., $k_{(\text{GEM+BrO})}/k_{(\text{GEM+Br})}$) still may be underestimated for the "BASE" simulation. For simulations "H_Br_L_BrO" and "L_Br_L_BrO", ΔGEM/ΔBrO was [greatly overestimated for O_3 levels below 10 ppb, which supports that $k_{(\text{GEM+BrO})}/k_{(\text{GEM+Br})}$ is underestimated for these simulations. The decrease in efficiency of GEM depletion by BrO for O_3 levels above ~30–40 ppbv, as observed in the "BASE" simulation, may be due to the predominance of O_3 over BrO in controlling GEM oxidation at high O_3 levels, which is further explored in Fig. 4.

Figure 4 explores relative contributions of BrO and O_3 to GEM depletions by plotting the ratio $\Delta\frac{\text{GEM\_O}_3}{\Delta t}/\Delta\frac{\text{GEM\_BrO}}{\Delta t}$ against O_3 for Julian day 201 using the "BASE" simulation. For O_3 levels above 30 ppbv, high ratios predominate, suggesting that for O_3 levels above ~30 ppbv, GEM oxidation is controlled predominantly by O_3. For O_3 levels below 30 ppbv, the ratios can be separated into ratios below and above 0.1; low ratios may be the expected result due to low O_3 availability. High ratios also occur, however, and these may be associated with time periods for which both BrO and O_3 concentrations

ACPD
11, 24467–24502, 2011

are low but O_3 shows a time delay in recovery after RBS activity is terminated toward late afternoon and evening.

3.3 Extent of GEM depletion

Br_2 release into the gas phase and subsequent BrO formation is dependent on meteorological conditions (Obrist et al., 2011), resulting in highly variable BrO diurnal profiles as shown in Fig. 5a, for all measured BrO during the campaign. As a result, O_3 and GEM depletions also show variable diurnal patterns (Fig. 5 b and c). Figure 5 also presents simulated diurnal profiles of O_3, BrO, and GEM for Julian days 188 and 201 with high and average BrOx levels, respectively. GEM levels at the Dead Sea rarely dropped below ~50 ppqv, and never below 22 ppqv, even when very high BrO levels were present (exceeding 100 pptv). This suggests that the efficiency of GEM depletion decreased at lower GEM, a notion supported in Fig. 3a. Figure 4 suggested that GEM depletion was controlled primarily by BrO_X at low O_3 levels (i.e., ~30–40 ppbv). Hence, reduced GEM depletion efficiency at lower GEM levels may be due to a decrease in BrO_X or GEM levels. Other reasons may include a decrease in photochemical oxidants such as O_3, HO_2O_2, and OH for lower GEM, associated with lower O_3 levels.

We further investigated dependence of the GEM depletion rate ($\Delta GEM/\Delta t$) as a function of BrO and GEM levels, both using days with low (Fig. 6a) and high (Fig. 6b) BrO levels. For high BrO_X levels ($> 6 \times 10^{-11}$ mol·mol^{-1}), our simulations suggested that $\Delta GEM/\Delta t$ was inversely related to GEM levels, and hence is strongly limited at low GEM (Fig. 6b insert; Julian day = 188). Figure 6b also suggests that the lifetime of GEM against oxidation by BrO_X decreased by about an order of magnitude for GEM levels above 4–24 $\times 10^{-14}$ mol × mol^{-1}, while no significant change in BrO (i.e., <10 %) occurred, suggesting that oxidation of GEM by BrO_X became GEM-limited and very inefficient below GEM concentrations of ~24 $\times 10^{-14}$. Alternatively, GEM oxidation by BrO_X became BrO_X-limited for BrO <~3 $\times 10^{-11}$ mol × mol^{-1} (Fig. 6a insert; Julian day = 201).

ACPD
11, 24467–24502, 2011

3.4 GEM oxidation pathways

The similarity in rate constants of the reactions of Br and BrO with GEM (Sect. 3.2) suggests that the role of BrO in GEM oxidation dominated over Br, as long as O_3 levels were not too low such that [BrO]/[Br] remained above 2. This is usually the case in the O_3-rich troposphere (Wayne et al., 1995).

Figure 7 shows calculated relative contributions of various oxidants to GEM depletion rates and associated GEM lifetimes, for Julian days 188 and 201 using the "BASE" simulation. This figure demonstrates that RBS (e.g., BrO, Br, and Br_2) and BrO_X contributed more than 90 % and 85 %, respectively, to GEM depletion on a 24-h basis for these days. Most of the GEM oxidation (>80 %) was caused by BrO, especially under lower BrO_X levels associated with higher O_3 levels and hence higher [BrO]/[Br] ratios. The associated diurnal average GEM lifetime against oxidation by BrO for Julian day 188 is 41.2 min, equivalent to a lifetime of 6.86 min for the daily peak BrO level of 90 ppt. Under lower BrO_X concentrations, the relative contributions of Br and Br_2 are comparable due to relatively higher [BrO]/[Br] ratios. The integrated sum contribution of NO_3, O_3, and OH was between ~4 and 8 % on a 24-h basis for these simulation days.

3.5 Temperature effects

Temperature can significantly influence the efficiency of GEM oxidation by RBS in the gaseous and aqueous phases. Temperature-dependencies for many mercury reactions are unknown, although the thermal back-dissociation of HgBr is known to significantly slow down GEM oxidation in the gas phase (Goodsite et al., 2004). Using rates given by Goodsite et al. (2004), the thermal back-dissociation of HgBr is ~2.6 orders of magnitude higher under the average Dead Sea summer temperature measured during the campaign (~310 k) compared to typical temperatures in the polar regions (240 k).

Figure 8 presents the GEM diurnal profile obtained for "BASE", "WINTER", and "POLAR" simulations in order to investigate temperature effects on GEM oxidation. Only direct effects of temperature on the Hg-involved chemical reactions were investigated,

ACPD
11, 24467–24502, 2011

while indirect effects of temperature – for instance, on the release of RBS into the gas phase (Sander et al., 2006) – were ignored here. Figure 8b demonstrates that under relatively moderate BrO levels such as on Julian day 201, temperature effects on the efficiency of GEM oxidation by RBS during AMDE were minimal, averaging ~16.8 % and continuously decreasing for lower GEM levels. Oxidation of GEM under typical polar temperatures were more efficient than for Dead Sea summer by 69.9 %, on average, but by only 27.6 % for low GEM concentrations. Figure 8a also shows that temperature effects were significantly lower under the high BrO_X levels observed on Julian day 188, where differences in GEM depletions averaged 10.9 % between typical Dead Sea summer and winter temperatures and 19.7 % between Dead Sea summer and polar temperatures. This is due, to a large extent, to the fact that GEM depletion becomes highly limited by the relatively low GEM concentrations, in the presence of high BrO_X concentrations (Sect. 3.3).

Obrist et al. (2011) showed that GEM depletions by BrO_X at the Dead Sea occurred even at low BrO concentrations between ~4 and 6 ppt (and possibly below), suggesting that this has important implications on Br-induced GEM depletions above oceans in the mid-latitudes and tropics. The present analysis indicates that GEM depletions in such areas is not expected to show high temperature dependency since at low BrO_X levels (e.g., BrO <~6.5 ppt [Saiz Lopez et al., 2004]), [BrO]/[Br] ratios are expected to be significantly larger than 2 (e.g., Fig. 3) and thus BrO becomes the predominant GEM oxidant.

3.6 Anthropogenic NO_x and SO_X

Anthropogenic pollution can directly enhance GEM depletion by oxidation by O_3, H_2O_2, and OH. The potential role of NO_3 in GEM oxidation outside of the polar regions has been addressed in several field measurement studies (e.g., Mao et al., 2008; Shon et al., 2005) and was shown by Mao et al. (2008) to be comparable or even higher than GEM oxidation by O_3, by using the upper limit of k_{Hg+NO3} (Sommar et al., 1997). Since significant conversion of NO_2 to nitrate can be associated with RBS activity (Tas et al.,

ACPD
11, 24467–24502, 2011

2006, 2008; Sander et al., 1999; Evans et al., 2003; Pszenny et al., 2004), enhanced nighttime GEM oxidation by NO_3 can occur in areas influenced by anthropogenic pollution, in addition to daytime RBS catalyzed GEM depletion.

NO_3 was not measured in the present study but has been detected at nighttime with up to levels of tens of ppt on a daily basis and up to ~300 ppt at the Dead Sea during summer (Peleg et al., unpublished data). High nighttime variance of GEM concentrations during the measurement campaign as seen in Fig. 5 may indicate the occurrence of GEM oxidation by elevated levels of NO_3. Assuming typical NO_3 concentrations of 50 ppt and $k_{Hg+NO3} = 4\times10^{-15}$ cm ^{3} molecule^{-1} s^{-1} (Sommar et al., 1997), the lifetime of GEM against oxidation by NO_3 is expected to be about 55 h, equivalent to a lifetime of ~6 days (using typical Dead Sea NO_3 diurnal profile). Figure 9 presents the diurnal time evolution of the relative contribution of different species to GEM oxidation for Julian day 188. The graph demonstrates that by applying NO_3 of ~20 ppt and k_{Hg+NO3} = 4×10^{-15} cm ^{3} molecule^{-1} s^{-1} nitrate was the predominant nighttime GEM oxidant, while Br_2 and O_3 were only of secondary importance. Figure 8 demonstrates that under moderate BrO_X loadings, the GEM depletion rate during "NOBROX" is much higher during nighttime compared to the "ONLYBR" simulation, due to oxidation by NO_3.

SO_2 can influence the oxidation rate of GEM indirectly by absorbance of aerosols to yield sulphite via the following reactions:

$$SO_2 \leftrightarrow SO_{2(aq)} \quad \text{(R1)}$$

$$SO_{2(aq)} \leftrightarrow HSO_3^- + H^+ \quad \text{(R2)}$$

$$HSO_{3\,(aq)}^- \leftrightarrow SO_3^{2-}{}_{(aq)} + H^+{}_{(aq)} \quad \text{(R3)}$$

The sulphite can then reduce Hg^{2+} and yield $Hg^{(0)}$ in the aqueous phase as follows:

$$Hg^{2+}_{(aq)} + SO_3^{2-}{}_{(aq)} \leftrightarrow HgSO_{3(aq)} \quad \text{(R4)}$$

$$HgSO_{3(aq)} + H_2O \rightarrow Hg^0{}_{(aq)} + HSO_{4\,(aq)}^- + H^+_{(aq)} \quad \text{(R5)}$$

ACPD
11, 24467–24502, 2011

Figure 8 investigates the influence of SO_2 on mercury oxidation by RBS and demonstrates that for Julian day 188, high levels of SO_2 led to lower rates of GEM oxidation in agreement with the above reactions (Fig. 8a). Conversely, Fig. 8b demonstrates that for relatively low BrO_X concentrations (Julian day 201), an increase in SO_2 concentration leads to an increase in the GEM oxidation rate, associated with an increase in BrO concentrations up to ~5 ppt. The increase in BrO concentrations results from an enhanced release rate of Br_2 into the gas phase, mainly from sulphate aerosols, caused by elevated $SO_{3\,(aq)}^{2-}$ levels according to the following reactions:

$$SO_{3(aq)}^{2-} + HOBr \rightarrow Br_{(aq)}^{-} + HSO_{4\,(aq)}^{-} \quad \text{(R6)}$$

$$BrONO_2 + Br_{(aq)}^{-} \rightarrow Br_2 + NO_3 \quad \text{(R7)}$$

4 Summary and conclusions

The present study demonstrated the high efficiency and central role of BrOx (a diurnal relative contribution of more than ~90 %) in AMDEs at the Dead Sea. BrO was found to be the dominant oxidant, with a diurnal relative contribution above ~80 %. In order to obtain good agreement between model simulations and observed GEM, k_{Hg+Br} and k_{Hg+BrO} depletion rates of 1.5×10^{-13} and $1. \times 10^{-13}$ cm ^{3} molecule^{-1} s^{-1}, respectively, had to be used. This indicates that BrO is the dominant GEM oxidant, for [BrO]/[Br] ratio above 2, which is usually the case in the O_3-rich troposphere.

Since under most conditions BrO is the predominant GEM oxidant, the proposed chemical mechanism causes GEM depletion to be very efficient under Dead Sea conditions, even though the reversible reaction of HgBr to yield back GEM is calculated to be faster by ~2.6 orders of magnitude at Dead Sea temperatures compared with the polar regions. The effect of temperature becomes significantly less important for higher BrO_X levels, mainly due to enhanced limitation of GEM depletion caused by its own decreasing concentrations. The analysis supports the prior conclusion (Obrist

ACPD
11, 24467–24502, 2011

et al., 2011) that Br-induced GEM depletion can be important above oceans in the mid-latitudes and tropics, even under relatively low BrO_X levels in these areas.

In addition to direct GEM oxidation by anthropogenic pollutants (e.g., O_3, H_2O_2, OH), there are several indirect pathways in which anthropogenic pollution can influence GEM oxidation. The interaction of NO_2 with BrO_X led to elevated NO_3 concentrations during the nighttime which can then cause significant GEM depletion even when averaged on a 24-hr basis. Increases in SO_2 concentration, and its subsequent uptake by aerosols, increased the formation rate of sulphite which in turn reduced the Hg^{II+} to GEM conversion rate in the aqueous phase, thereby reducing the overall rate of GEM depletion. Conversely, under relatively lower BrO_X concentrations (e.g., <30 ppt), increases in the SO_2 concentration can lead to an increase in GEM depletion by enhancing the rate of Br_2 release, due to an increase in the conversion of HOBr into Br^-(aq) by the sulphite.

Under the relatively high Dead Sea BrO levels, GEM depletion is limited to levels of ~25 ppqv and becomes significantly inefficient below ~50 ppqv, due to the fact that further GEM depletion becomes highly dependent on its own concentration.

Supplementary material related to this article is available online at: http://www.atmos-chem-phys-discuss.net/11/24467/2011/acpd-11-24467-2011-supplement.pdf.

Acknowledgements. We thank R. Sander for use of the MECCA model; the Dead Sea Works for site logistics; J. Zingler, J. Lenvant, and U. Corsmeier for meteorological data; The study was funded by the US National Science Foundation (no. 0813690 to D.O. and M.L.), and has benefited from a US Environmental Protection Agency Star-to-Achieve grant (R833378).

References

Ariya, P. A., Khalizov, A., and Gidas, A.: Reaction of gaseous mercury with atomic and molecular halogens: Kinetics, product studies, and atmospheric implications, J. Phys. Chem. A, 106, 7310–7320, 2002.

ACPD
11, 24467–24502, 2011

Ariya, P., Dastoor, A., Amyot, M., Schroeder, W.H., Barrie, L., Anlauf, K., Raofie, F., Ryzhkov, A., Davignon, D., Lalonde, J., Steffen, A.: The Arctic: A sink for mercury, Tellus, 56B, 397–403, 2004.

Ariya, P. A., Skov, H., Grage, M. M. L., and Goodsite, M. E.: Gaseous elemental mercury in the ambient atmosphere: Review of the application of theoretical calculations Fig. 2. Calculated and experimental studies for determination of reaction coefficients and mechanisms with halogens and other reactants. Advances in Quantum Chemistry: Applications of Theoretical Methods to Atmospheric, Science 55, 43–55, 2008.

Aspmo, K., Gauchard, P.-A., Steffen, A., Temme, C., Berg, T., Bahlmann, E., Banic, C., Dommergue, A., Ebinghaus, R., Ferrari, C., Pirrone, N., Sprovieri, F., and Wibetoe, G.: Measurements of atmospheric mercury species during an international study of mercury depletion events at Ny-A lesund, Svalbard, spring 2003, How reproducible are our present methods?, Atmos. Environ., 39, 7607–7619, 2005.

Berg, T., Sekkesæter, S., Steinnes, E., Valdal, A.-K., and Wibetoe, G.: Springtime depletion of mercury in the European Arctic as observed at Svalbard, Sci. Total Environ., 304, 43–51, 2003.

Bergan, T. and Rodhe, H.: Oxidation of elemental mercury in the atmosphere: Constraints imposed by global scale modeling, J. Atmos. Chem., 40, 191–212, 2001.

Bottenheim, J. W., Gallant, A. C., and Brice, K. A.: Measurements of NOy species and O_3 at 2° N latitude, Geophys. Res. Lett., 1986, 13, 113–116, 1986.

Brooks, S., Saiz-Lopez, A., Skov, H., Lindberg, S., Plane, J., and Goodsite, M.: The mass balance of mercury in the springtime Arctic environment, Geophys. Res. Lett., 33, L13812, doi:10.1029/2005GL025525, 2006.

Byun, Y., Cho, M., Namkung, W., Lee, K., Koh, D. J., and Shin, D. N.: Insight into the Unique Oxidation Chemistry of Elemental Mercury by Chlorine-Containing Species: Experiment and Simulation, Environ. Sci. Technol., 2010, 44, 1624–1629, 2010.

Calvert, J. G. and Lindberg, S. E.: A modeling study of the mechanism of the halogen-ozone-mercury homogeneous reactions in the troposphere during the polar spring, Atmos. Environ., 37, 4467–4481, 2003.

Calvert, J. G. and Lindberg, S. E.: The potential influence of iodine-containing compounds on the chemistry of the troposphere in the polar spring: II. Mercury depletion, Atmos. Environ., 38, 5105–5116, 2004.

Clever, H., Johnson, S. A., and Derrick, E. M.: The solubility of mercury and some sparingly

ACPD
11, 24467–24502, 2011

soluble mercury salts in water and aqueous solutions, J. Phys. Chem. Ref. Data., 14, 631–680, 1985.

Donohoue, D. L., Bauer, D., Cossairt, B., and Hynes, A. J.: Temperature and pressure dependent rate coefficients for the reaction of Hg with Br and the reaction of Br with Br: a pulsed laser photolysis-pulsed laser induced fluorescence study, J. Phys. Chem. A, 110, 6623–6632, 2006.

Driscoll, C. T., Han, Y. J., Chen, C. Y., Evers, D. C., Lambert, K. F., Holsen, T. M., Kamman, N. C., and Munson, R. K.: Mercury contamination in forest and freshwater ecosystems in the northeastern United States, Bioscience, 57(1), 17–28, 2007.

Ebinghaus, R., Jennings, S. G., Schroeder, W., Berg, T., Donaghy, T., Guentzel, J., Kenny, C., Kock, H. H., Kvietkus, K., Landing, W., Mühleck, T., Munthe, J., Prestbo, E. M., Schneeberger, D. R., Slemr, F., Sommar, J., Urba, A., Wallschläger, D., and Xiao, Z.: International field inter-comparison measurements of atmospheric mercury species at Mace Head, Ireland, Atmos. Environ., 33, 3063–3073, 1999.

Ebinghaus, R., Kock, H. H., Temme, C., Einax, J. W., Löwe, A. G., Richter, A., Burrows, J. P., and Schroeder, W. H.: Antarctic springtime depletion of atmospheric mercury, Environ. Sci. Technol., 36, 1238–1244, 2002.

Evans, M. J., Jacob, D. J., Atlas, E., Cantrell, C. A., Eisele, F., Flocke, F., Fried, A., Mauldin, R. L., Ridley, B. A., Wert, B., Talbot, R., Blake, D., Heikes, B., Snow, J., Welega, J., Weinheimer,A. J., and Dibb, J.: Coupled evolution of BrO_X-ClOXHOX-NO_X chemistry during bromine-catalyzed ozone depletion events in the Arctic boundary layer, J. Geophys. Res., 108(D4), 8368, doi:10.1029/2002JD002732, 2003.

Gong, S. L., Barrie, L. A., and Blachey, J.-P.: Modelling sea-salt aerosols in the atmosphere, 1. Model development, J. Geophys. Res., 102(D3), 3805–3818, 1997.

Goodsite, M., Plane, J. M. C., and Skov, H.: A theoretical study of the oxidation of Hg° to $HgBr_2$ in the troposphere, Environ. Sci. Technol., 38, 1772–1776, 2004.

Hebestreit, K., Stutz, J., Rosen, D., Matveev, V., Peleg, M., Luria, M., and Platt, U.: First DOAS Measurements of Tropospheric Bromine Oxide in Mid Latitudes, Science, 283, 55–57, 1999.

Hedgecock, I. M. and Pirrone, N.: Mercury and photochemistry in the marine boundary layer-modelling studies suggest the in situ production of reactive gas phase mercury, Atmos. Environ., 35, 3055–3062, 2001.

Hedgecock, I. M. and Pirrone, N.: Chasing quicksilver: Modeling the atmospheric lifetime of Hg0 (g) in the marine boundary layer, Environ. Sci. Technol., 38, 69–76, 2004.

ACPD
11, 24467–24502, 2011

Hedgecock, I. M. and Pirrone, N.: Chasing quicksilver: Modeling the atmospheric lifetime of Hg0 (g) in the marine boundary layer at various latitudes, Environ. Sci. Technol., 38, 69–76, 2004.
Hedgecock, I. M., Pirrone, N., Sprovieri, F., and Pesenti, E.: Reactive gaseous mercury in the marine boundary layer: Modeling and experimental evidence of its formation in the Mediterranean region, Atmos. Environ., 37, S41–S49, 2003.
Hedgecock, I. M., Trunfio, G. A., Pirrone, N., and Sprovieri, F.: Mercury chemistry in the MBL: Mediterranean case and sensitivity studies using the AMCOTS (Atmospheric Mercury Chemistry over the Sea) model, Atmos. Environ., 39, 7217–7230, 2005.
Hedgecock, I. M., Pirrone, N., and Sprovieri, F.: Chasing quicksilver northward: Mercury chemistry in the Arctic troposphere, Environ. Chem., 5, 131–134, 2008.
Holmes, C. D., Jacob, D. J., and Yang, X.: Global lifetime of elemental mercury against oxidation by atomic bromine in the free troposphere, Geophys. Res. Lett., 33, L20808, doi:10.1029/2006GL027176, 2006.
Holmes C. D., Jacob D. J., Mason R. P., and Jaffe D. A.: Sources and deposition of reactive gaseous mercury in the marine atmosphere, Atmos. Environ., 43, 2278–85, 2009.
Karg, E., Uhl, J., and Heyder, J.: Particle Density of Sulfite and Sulfate Test Aerosols, J. Aerosol Sci., 26, S611–S612, 1995.
Kerkweg, A., Sander, R., Tost, H., Jöckel, P., and Lelieveld, J.: Technical Note: Simulation of detailed aerosol chemistry on the global scale using MECCA-AERO, Atmos. Chem. Phys., 7, 2973–2985, doi:10.5194/acp-7-2973-2007, 2007.
Landgraf, J. and Crutzen, P. J.: An efficient method for online calculations of photolysis and heating rates, J. Atmos. Sci., 55(5), 863–878, 1998.
Landis, M. S., Stevens, R. K., Schaedlich, F., and Prestbo, E. M.: Development and characterization of an annular denuder methodology for the measurement of divalent inorganic reactive gaseous mercury in ambient air, Environ. Sci. Technol., 36(13), 3000–3009, 2002.
Lin, C.-J. and Pehkonen, S. O.: Aqueous free radical chemistry of mercury in the presence of iron oxides and ambient aerosol, Atmos. Environ., 31, 4125–4137, 1997.
Lin, C.-J. and Pehkonen, S. O.: Oxidation of elemental mercury by aqueous chlorine (HOCl/OCl-): Implications for tropospheric mercury chemistry, J. Geophys. Res., 103D, 28093–28102, 1998.
Lin, C.-J. and Pehkonen, S. O.: Aqueous phase reactions of mercury with free radicals and chlorine: Implications for atmospheric mercury chemistry, Chemosphere, 38, 1253–1263,

ACPD
11, 24467–24502, 2011

1999.
Lin, C.-J., Pongprueksa, P., Lindberg, S. E., Pehkonen, S. O., Byune, D., and Jang, C.: Scientific uncertainties in atmospheric mercury models I: Model science evaluation, Atmos. Environ., 40, 2911–2928, 2006.
Lindberg, S. E., Brooks, S., Lin, C.-J., Scott, K., Meyers, T., Chambers, L., Landis, M., and Stevens, R. K.: Formation of Reactive Gaseous Mercury in the Arctic: Evidence of Oxidation of Hg to Gas-Phase Hg-II Compounds after Arctic Sunrise, Water Air Soil Pollut., 1(5–6), 295–302, 2001.
Lindberg, S. E., Brooks, S., Lin, C.-J., Scott, K. J., Landis, M. S., Stevens, R. K., Goodsite, M., and Richter, A.: Dynamic oxidation of gaseous mercury in the Arctic troposphere at polar sunrise, Environ. Sci. Technol., 36, 1245–1256, 2002.
Lu, J. Y., Schroeder, W. H., Barrie, L. A., and Steffen, A.: Magnification of atmospheric mercury deposition to polar regions in springtime: The link to tropospheric ozone depletion chemistry, Geophys. Res. Lett. 28, 3219–3222, 2001.
Mao, H., Talbot, R. W., Sigler, J. M., Sive, B. C., and Hegarty, J. D.: Seasonal and diurnal variations of Hg over New England, Atmos. Chem. Phys., 8, 1403–1421, doi:10.5194/acp-8-1403-2008, 2008.
Matveev, V., Peleg, M., Rosen, D., Tov-Alper, D. S., Hebestreit, K., Stutz, J., Platt, U., Blake, D., and Luria, M.: Bromine oxide-ozone interactions over the Dead Sea, J. Geophys. Res, 106, 10375–10387, 2001.
McNider, R. T. and Pielke, R. A.: Diurnal boundary-layer development over sloping terrain, J. Atmos. Sci., 38, 2198–2212, 1981.
Munthe, J.: The aqueous oxidation of elemental mercury by ozone, Atmos. Environ. Part A-General Topics, 26(8), 1461–1468, 1992.
Niki, H., Maker, P. D., Savage, C. M., and Breithnbach, L. P.: A long-path Fourier transform study of the kinetics and mechanism for the HO-radical initiated oxidation of dimethyl mercury, J. Phys. Chem, 87, 4978–4981, 1983b.
Obrist, D., Tas, E., Peleg, M., Matveev, V., Faïn, X., Asaf, D., and Luria, M.: Bromine-induced oxidation of mercury in the mid-latitude atmosphere, Nature Geosci., 4, 22–26, 2011.
Pal, B. and Ariya, P. A.: Gas-phase HO-initiated reactions of elemental mercury: Kinetics, product studies, and atmospheric implications, Environ. Sci. Technol., 38, 5555–5566, 2004a.
Pal, B. and Ariya, P. A.: Studies of ozone initiated reactions of gaseous mercury: Kinetics, product studies, and atmospheric implications, Phys. Chem. Chem. Phys., 6, 572–579, 2004b.

ACPD
11, 24467–24502, 2011

Pehkonen, S. O. and Lin, C.-J.: Aqueous photochemistry of mercury with organic acids, J. Air. Waste. Manage., 48, 144–150, 1997.
Peleg, M., Matveev, V., Tas, E., and Luria, M.: Mercury Depletion Events in the Troposphere in Mid-Latitudes at the Dead Sea, Israel. Environ. Sci. Technol., 41, 7280–7285, 2007.
Petersen, G., Munthe, J., Pleijel, K., Bloxam, R., and Kumar, A. V.: A comprehensive Eulerian modeling framework for airborne mercury species: Development and testing of the tropospheric chemistry module (TCM), Atmos. Environ., 32, 829–843, 1998.
Pleijel, K. and Munthe, J.: Modelling the atmospheric mercury cy-cle – -chemistry in fog droplet, Atmos. Environ., 29, 1441–1457, 1995.
Poissant, L. and Pilote, M.: Time series analysis of atmospheric mercury in Kuujjuarapik/Whapmagoostui (Québec), J. Phys. IV France, 107, 1079–1082, 2003.
Pszenny, A. A. P., Moldanov, J., Keene, W. C., Sander, R., Maben, J. R., Martinez, M., Crutzen, P. J., Perner, D., and Prinn, R. G.: Halogen cycling and aerosol pH in the Hawaiian marine boundary layer, Atmos. Chem. Phys., 4, 147–168, doi:10.5194/acp-4-147-2004, 2004.
Raofie, F. and Ariya, P. A.: Kinetics and products study of the reaction of BrO radicals with gaseous mercury, J. Phys. IV France, 107, 1119–1121, 2003.
Raofie, F., Snider, G., and Ariya, P. A.: Departments of Chemistry and Atmospheric and Oceanic Sciences, McGill University, 801 Sherbrooke St. W., Montreal, QC H3A 2K6, Canada, 2008.
Saiz-Lopez, A., Plane, J. M. C., and Shillito, J. A.: Bromine oxide in the mid-latitude marine boundary layer, Geophys. Res. Lett., 31(3), L03111, 2004.
Sander, R., Rudich, Y., von Glasow, R., and Crutzen., P. J.: The role of $BrNO_3$ in marine tropospheric chemistry: A model study, Geophys. Res. Lett., 26(18), 2857–2860, 1999.
Sander, R., Kerkweg, A., Jöckel, P., and Lelieveld, J.: Technical note: The new comprehensive atmospheric chemistry module MECCA, Atmos. Chem. Phys., 5, 445–450, doi:10.5194/acp-5-445-2005, 2005.
Sander, R., Burrows, J., and Kaleschke, L.: Carbonate precipitation in brine - a potential trigger for tropospheric ozone depletion events, Atmos. Chem. Phys., 6, 4653–4658, doi:10.5194/acp-6-4653-2006, 2006.
Schroeder, W. H. and Munthe, J.: Atmospheric mercury – An overview. Atmos. Environ., 32, 809–822, 1998.
Schroeder, W. H., Yarwood, G., and Niki, H.: Transformation processes involving mercury species in the atmosphere – Results from a literature survey, Water Air Soil Poll., 56, 653–

ACPD
11, 24467–24502, 2011

666, 1991.
Schroeder, W. H., Keeler, G., Kock, H., Roussel, P., Schneeberger, D., and Schaedlich, F.: International field inter-comparison of atmospheric mercury measurement methods, Water Air Soil Poll., 80, 611–620, 1995.
Schroeder, W. H., Anlauf, K. G., Barrie, L. A., Lu, J. Y., Steffen, A., Schneeberger, D. R., and Berg, T.: Arctic springtime depletion of mercury, Nature, 394, 331–332, 1998.
Seigneur, C., Wrobel, J., Constantinou, E., Gillespie, P., Bergstrom, R. W., Sykes, I., Venkatram, A., ad Karamchandani, P. A.: Chemical kinetic mechanism for atmospheric inorganic mercury, Environ. Sci. Technol., 28, 1589–1597, 1994.
Shepler, B. C., Balabanov, N. B., and Peterson, K. A.: Hg+Br!HgBr recombination and collision-induced dissociation dynamics, J. Chem. Phys., 127, 164–304, doi:10.1063/1.2777142, 2007.
Shon, Z.-H., Kim, K.-H., Kim, M.-Y. and Lee, M.: Modeling study of reactive gaseous mercury in the urban air, Atmos. Environ., 39, 749–761, 2005.
Sillman, S., Marsik, F. J., Al-Wali, K. I., Keeler, G. J., and Landis, M. S.: Reactive mercury in the troposphere: Model formation and results for Florida, the northeastern United States, and the Atlantic ocean, J. Geophys. Res., 112, D23305, doi:10.1029/2006JD008227, 2007.
Skov, H., Christensen, J. H., Goodsite, M. E., Heidam, N. Z., Jensen, B., Wahlin, P., and Geernaert, G.: Fate of elemental mercury in the Arctic during atmospheric mercury depletion episodes and the load of atmospheric mercury to the Arctic, Environ. Sci. Technol., 38, 2373–2382, 2004.
Smith, R. M. and Martell, A. E.: Critical stability constants Inorganic Complexes, 4, Plenum, New York, USA, 1976.
Smoydzin, L. and von Glasow, R.: Modelling chemistry over the Dead Sea: bromine and ozone chemistry, Atmos. Chem. Phys., 9, 5057–5072, doi:10.5194/acp-9-5057-2009, 2009.
Sommar, J., Hallquist, M., Ljungstrom E., and Lindqvist, O.: On the gas phase reactions between volatile biogenic mercury species and the nitrate radical, J. Atmos. Chem., 27, 233–247, 1997.
Sommar, J., Wängberg, I., Berg, T., Gårdfeldt, K., Munthe, J., Richter, A., Urba, A., Wittrock, F., and Schroeder, W. H.: Circumpolar transport and air-surface exchange of atmospheric mercury at Ny-Ålesund (79° N), Svalbard, spring 2002, Atmos. Chem. Phys., 7, 151–166, doi:10.5194/acp-7-151-2007, 2007.
Spivakovsky, C. M., Logan, J. A., Montzka, S. A., Balkanski, Y. J., Foreman-Fowler, M., Jones,

ACPD
11, 24467–24502, 2011

D. B. A., Horowitz, L.W., Fusco, A. C., Brenninkmeijer, C. A. M., Prather, M. J., Wofsy, S. C., and McElroy, M. B.: Three-dimensional climatological distribution of tropospheric OH: Update and evaluation, J. Geophys. Res., 105, 8931–8980, doi:10.1029/1999JD901006, 2000.

Stutz, J. and Platt, U.: Numerical analysis and estimation of the statistical error of differential optical absorption spectroscopy measurements with least-squares methods, Appl. Optics, 35(30), 6041–6053, 1996.

Tas, E., Peleg, M., Matveev, V., Zingler, J., and Luria, M.: Frequency and extent of bromine oxide formation over the Dead Sea, J. Geophys. Res., 110(D11), D11304, doi:10.1029/2004JD005665, 2005.

Tas, E., Peleg, M., Pedersen, D. U., Matveev, V., Pour Biazar, A., and Luria, M.: Measurement-based modeling of bromine chemistry in the boundary layer: 1. Bromine chemistry at the Dead Sea, Atmos. Chem. Phys., 6, 5589–5604, doi:10.5194/acp-6-5589-2006, 2006.

Tas, E., Peleg, M., Pedersen, D. U., Matveev, V., Biazar, A. P., and Luria, M.: Measurement-based modeling of bromine chemistry in the Dead Sea boundary layer – Part 2: The influence of NO_2 on bromine chemistry at mid-latitude areas, Atmos. Chem. Phys., 8, 4811-4821, doi:10.5194/acp-8-4811-2008, 2008.

Tokos, J. J. S., Hall, B., Calhoun, J. A., and Prestbo, E. M.: Homogeneous gas-phase reaction of Hg0 with H2O2, O3, CH3I, and (CH3)2S: Implications for atmospheric Hg cycling, Atmos. Environ., 32, 823–827, 1998.

Tossell, J. A.: Calculation of the energetics for oxidation of gas-phase elemental Hg by Br and BrO, Phys. Chem. A, 107, 7804–7808, 2003.

Tossell, J. A.: Calculation of the energetics for the oligomerization of gas phase HgO and HgS and for the solvolysis of crystalline HgO and HgS, J. Phys. Chem. A, 110, 2571–2578, 2006.

Van Loon, L., Mader, E., and Scott, S. L.: Reduction of the aqueous mercuric ion by sulfite: UV spectrum of $HgSO_3$ and its intra-molecular redox reaction, J. Phys. Chem. A, 104, 1621–1626, 2000.

Van Loon, L. L., Mader, E. A., and Scott, S. L.: Sulfite stabilization and reduction of the aqueous mercuric ion: Kinetic determination of sequential formation constants, Phys. Chem. A, 105, 3190–3195, 2001.

Wang, Z. and Pehkonen, S. O.: Oxidation of elemental mercury by aqueous bromine: Atmospheric implications, Atmos. Environ., 38, 3675–3688, 2004.

Xiao, Z. F., Munthe, J., Stromberg, D., and Lindqvist, O.: Photochemical behavior of inorganic mercury compounds in aqueous solution, in: Mercury as a Global Pollutant – Integration and

ACPD
11, 24467–24502, 2011

Synthesis, edited by: Watras, C. J. and Huckabee, J. W., 581–592, Lewis Publishers, 1994.
Xie, Z.-Q., Sander, R., Pöschl, U., and Slemr, F.: Simulation of atmospheric mercury depletion events (AMDEs) during polar springtime using the MECCA box model, Atmos. Chem. Phys., 8, 7165–7180, doi:10.5194/acp-8-7165-2008, 2008.
Yue, G. K.: On the Characteristics of Sulfate Aerosols formed in the Presence of Ion Sources, J. Aerosol Sci., 10, 387–393, 1979.
Wayne, R. P., Poulet, G., Biggs, P., Burrows, J. P., Cox, R. A., Crutzen, P. J., Haymann, G. D., Jenkin, M. E., Bras, G. L., Moortgat, G. K., Platt, U., and Schindler, R. N.: Halogen oxides: Radicals, sources and reservoirs in the laboratory and in the atmosphere, Atmos. Environ., 29, 2675–2884, 1995.
Zingler, J. and Platt, U.: Iodine oxide in the Dead Sea Valley: Evidence for inorganic sources of boundary layer IO, J. Geophys. Res., 110, D07307, doi:10.1029/2004JD004993, 2005.

ACPD
11, 24467–24502, 2011

Table 1. Key to different simulation types. Simulations 1–4 were performed for four different days from the measurement campaign (Julian days 188, 197, 198, and 201) using different combinations for the rate of Hg with Br and BrO: low and high k_{Hg+Br} (=and cm^3 $molecule^{-1}$ s^{-1}) for "L_Br" and "H_Br," respectively, based on Donohoue et al. (2006) and Goodsite et al. (2004); k_{Hg+BrO} = and for "L_BrO" and "M_BrO," respectively, based on Raofie and Ariya (2003); and $k_{Hg+BrO} = 1.5. \times^{-13}$ cm^3 $molecule^{-1}$ s^{-1} for "H_BrO". L_Br_H_BrO," is referred to as "BASE" simulation due to best agreement with measurements. All simulations were performed for Julian days 188 and 201 which represent typical days of relatively high Dead Sea BrO levels (see additional details in Sect. 3.1).

Number	Simulation	Individual conditions for calculations
1	L_Br_H_BrO / BASE	Low and high k_{Hg+Br} and k_{Hg+BrO}, respectively
2	L_Br_M_BrO	Low and medium k_{Hg+Br} and k_{Hg+BrO}, respectively
3	L_Br_L_BrO	Low k_{Hg+Br} and k_{Hg+BrO}
4	H_Br_L_BrO	High and low k_{Hg+Br} and $k_{Hg+BrO,}$ respectively
5	L_Br_H_BrO_HgOp	Similar to BASE with higher $[HgO_{(p)}]/[HgO_{(g)}]$
6	NOBROX	Similar to BASE, not including BrO_X as GEM oxidants
7	ONLYBROX	Similar to BASE, including only BrO_X as GEM oxidants
8	ONLYBR	Similar to BASE, including only Br as GEM oxidants
9	$HIGHSO_2$	Similar to BASE, with higher SO_2 levels
10	WINTER	Similar to BASE, with GEM chemistry based on winter Dead Sea temperatures (averaged at ~294 k)
11	POLAR	Similar to BASE, with GEM chemistry based on polar regions temperatures (averaged at 240 k)

ACPD
11, 24467–24502, 2011

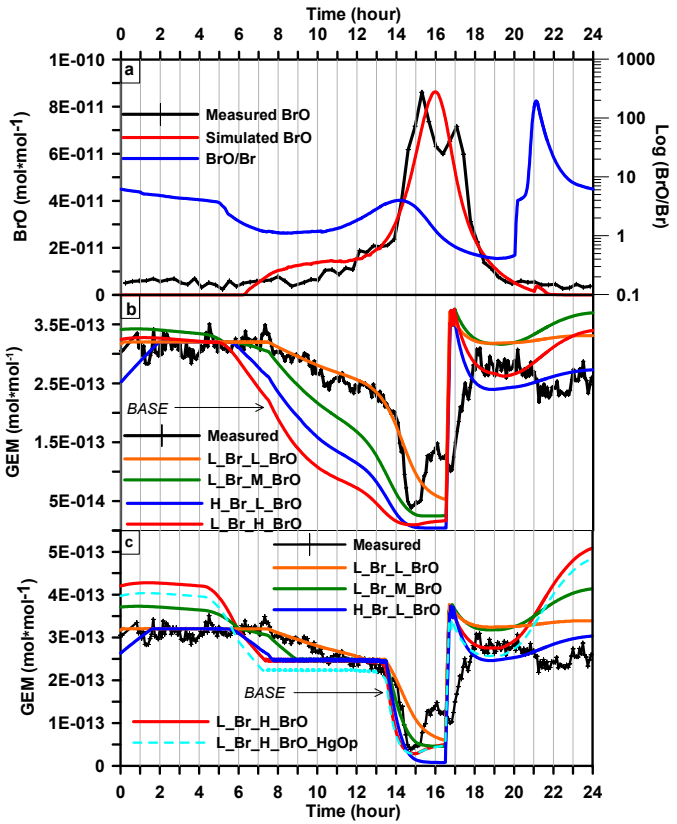

Fig. 1. Simulated vs. measured diurnal profiles of GEM and BrO. **(a)** Measured and simulated diurnal profiles of BrO, and simulated diurnal profile of [BrO]/[Br] for Julian day 188. **(b)** GEM diurnal profiles for different combinations of $k_{-\mathrm{GEM+BrO}}$ and $k_{-\mathrm{GEM+Br}}$ values (see Sect. 2.3). **(c)** Same as **(b)** with simulated GEM concentrations being constrained between 07:30 and 13:30 LT (Sect. 3.2).

ACPD
11, 24467–24502, 2011

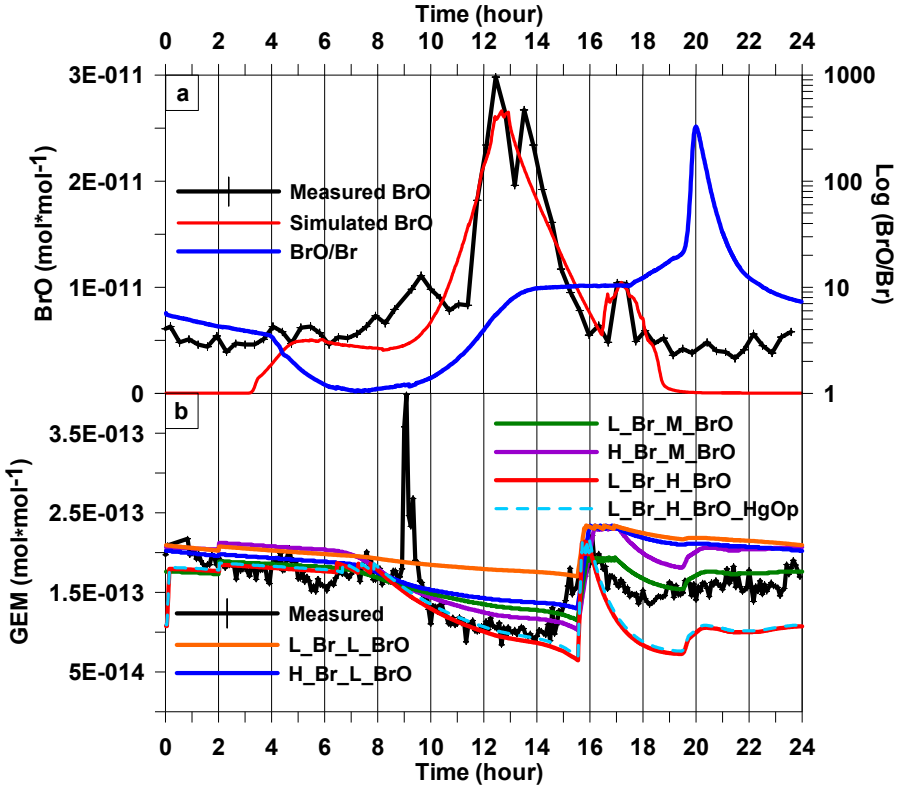

Fig. 2. Simulated vs. measured diurnal profiles of GEM and BrO. **(a)** Measured and simulated diurnal profiles of BrO and simulated diurnal profile of [BrO]/[Br] for Julian day 201. **(b)** Different combinations of values for $k_{-GEM+BrO}$ and $k_{-GEM+Br}$ were used to evaluate the simulated GEM diurnal profiles (see Sect. 2.3).

ACPD
11, 24467–24502, 2011

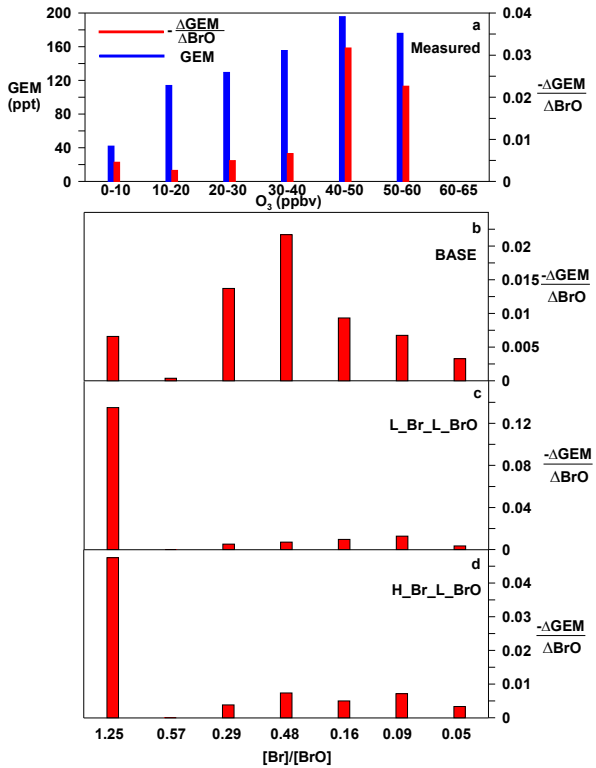

Fig. 3. The relative influence of Br and BrO on GEM oxidation. **(a)** Measured GEM depletion per BrO (ΔGEM/ΔBrO) as a function of O_3. ΔGEM/ΔBrO was calculated for all campaign days and averaged for respective O_3 values. **(b–d)** Simulated ΔGEM/ΔBrO as a function of [Br]/[BrO] for simulations L_Br_H_BrO (i.e., "BASE"; b), L_Br_L_BrO **(c)**, and H_Br_L_BrO **(d)**. Measured O_3 corresponds to [Br]/[BrO] ratios in simulations due to known positive correlations between the two. Simulated ΔGEM/ΔBrO values were calculated only for periods of ΔBrO > 0 and are based on Julian days 188, 197, 198, and 201.

ACPD
11, 24467–24502, 2011

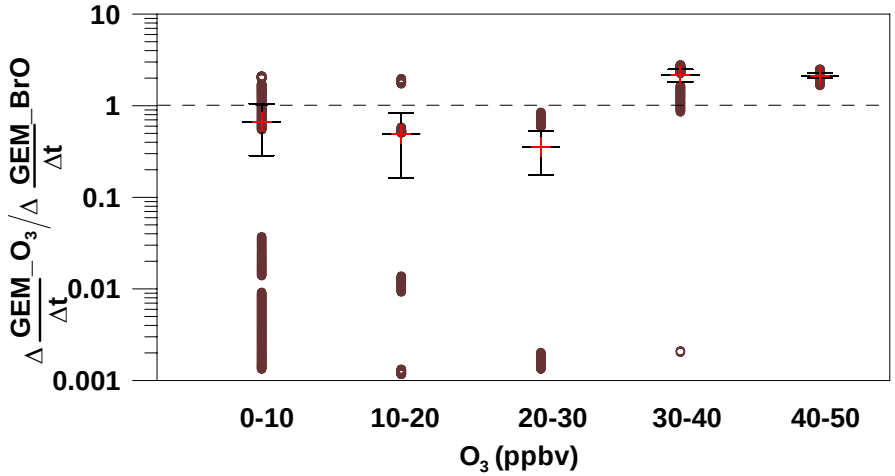

Fig. 4. The relative influence of O_3 and BrO on GEM depletion as a function of O_3 levels. Ratio of contributions of O_3 and BrO to GEM depletion, $\Delta \frac{GEM\_O_3}{\Delta t} / \Delta \frac{GEM\_BrO}{\Delta t}$, for Julian day 201 using "BASE" simulation are presented. Crosses represent the average values of all time increments, and horizontal lines below and above the averages represent 0.5 standard deviations.

ACPD
11, 24467–24502, 2011

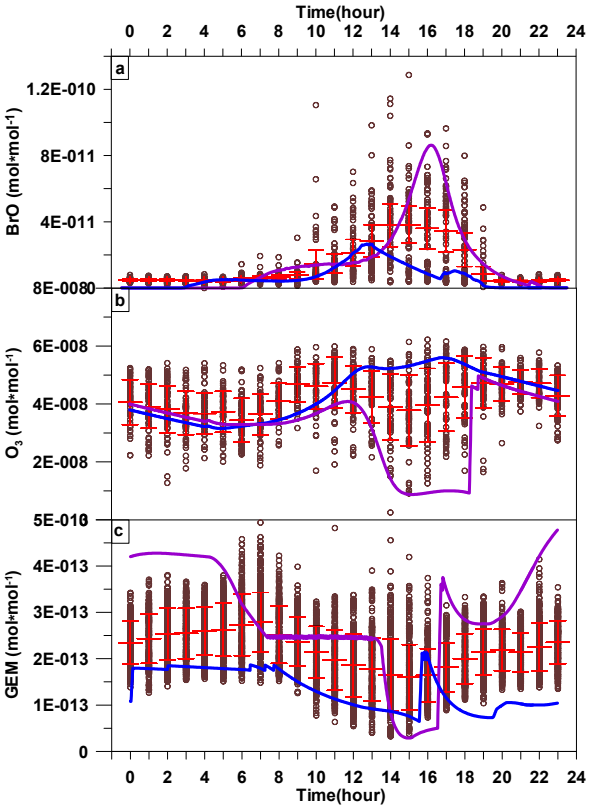

Fig. 5. Measured and simulated diurnal profiles of GEM, BrO, and O_3. Measured data points of entire campaign are plotted as dots. Crosses represent average concentrations for each hour, and horizontal lines below and above represent 0.5 standard deviations. Simulated BrO, O_3, and GEM are presented for Julian days 188 (pink line; high RBS day) and 201 (blue line; average RBS day) using the "BASE" simulation.

ACPD
11, 24467–24502, 2011

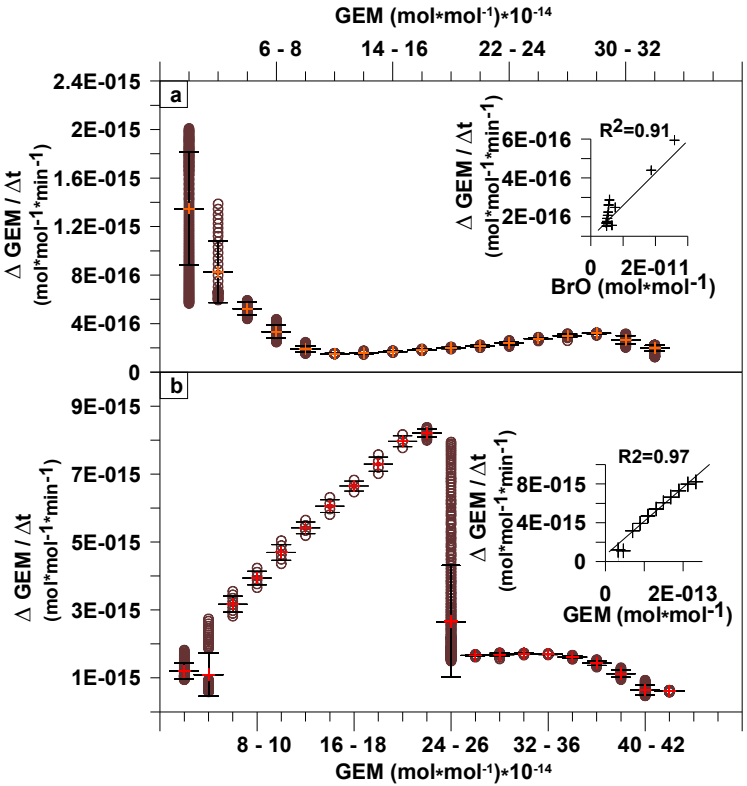

Fig. 6. Decrease in GEM depletion efficiency during AMDE. Efficiency of GEM depletion ($\Delta GEM/\Delta t$) graphed as a function of GEM for Julian days 201 (**(a)**; low BrOx day) and 188 (**(b)**; high BrOx day), using the "BASE" simulation. Figure inserts show modeled correlation of to BrO and GEM, respectively.

ACPD
11, 24467–24502, 2011

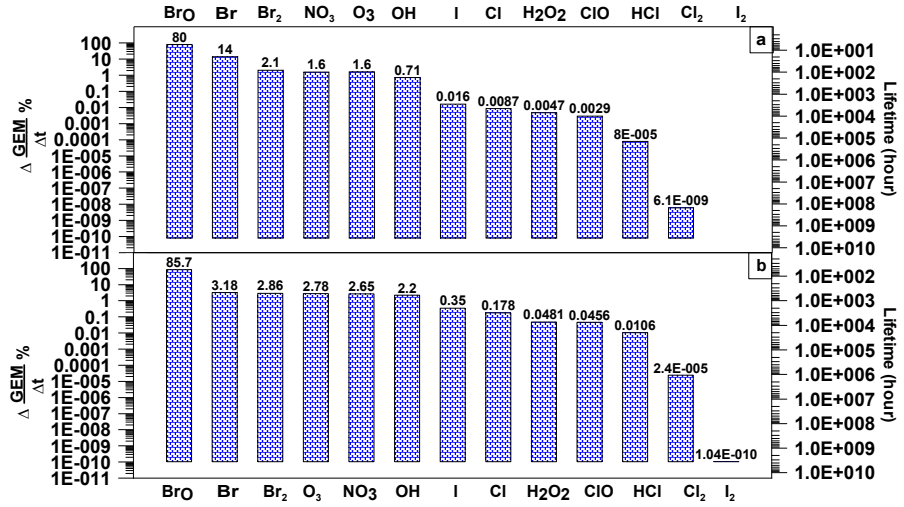

Fig. 7. Relative contributio %) of different species to GEM oxidation and associated GEM lifetimes for Julian days 188 **(a)** and 201 **(b)**, based on "BASE" simulation. Maximal concentrations of 20 ppt were used for NO_3.

ACPD
11, 24467–24502, 2011

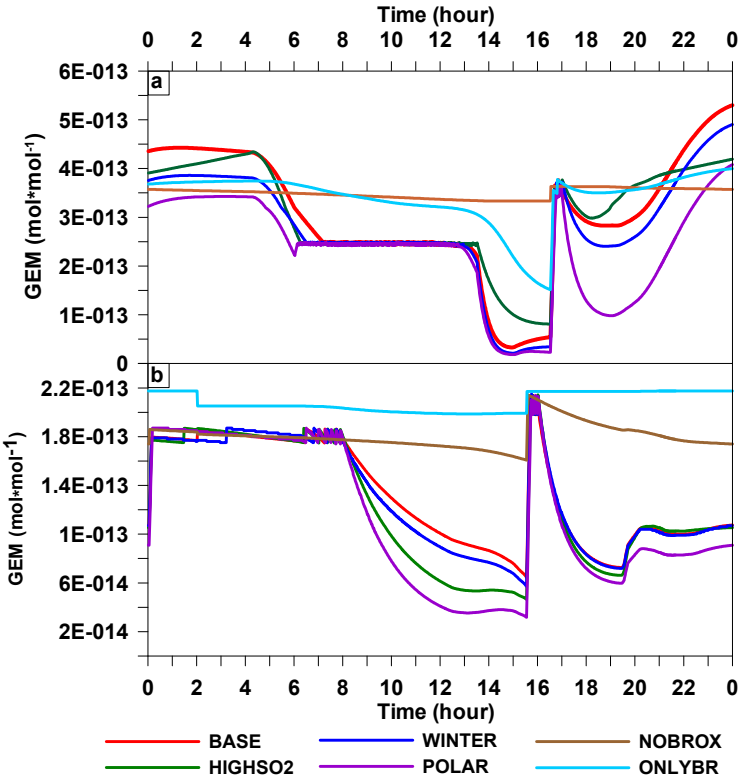

Fig. 8. Influence of BrO_X and temperature on GEM depletion. The influence of BrO_X, temperature and SO_2 on GEM depletion rate. The GEM diurnal profiles are shown for the "BASE", "$HIGHSO_2$", "WINTER", "POLAR", "NOBROX", and "ONLYBR" simulations (Sect. 2.3) for Julian days 188 **(a)** and 201**(b)**.

ACPD
11, 24467–24502, 2011

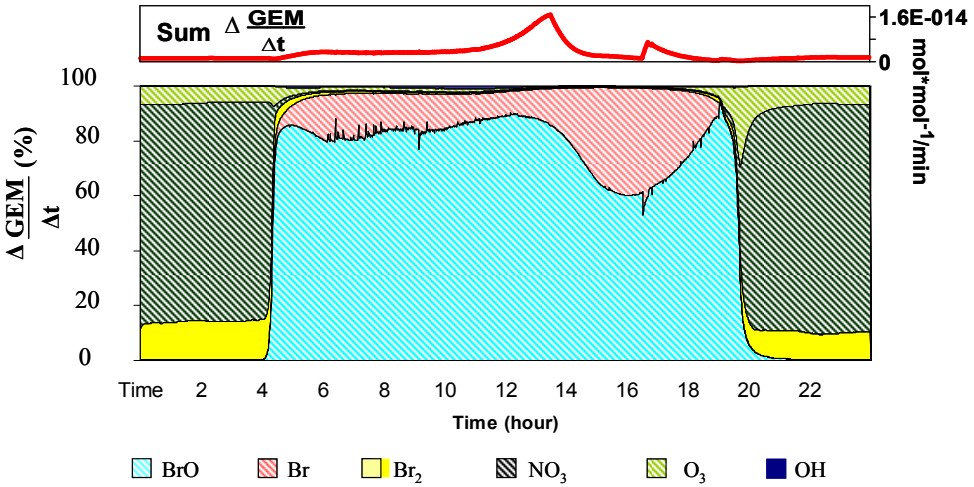

Fig. 9. Diurnal time evolution of GEM oxidation by the main oxidants. The simulated diurnal profiles of relative (in %) GEM depletion ($\frac{\Delta GEM}{\Delta t}$) caused by different oxidants, presented for Julian day 188.

ACPD
11, 24467–24502, 2011